ARTICLE IN PRESS

INTERNATIONAL JOURNAL OF HYDROGEN ENERGY XXX (XXXX) XXX

Available online at www.sciencedirect.com

ScienceDirect

journal homepage: www.elsevier.com/locate/he

How to achieve the Fleischmann-Pons heat effect

M.R. Staker

Department of Engineering, Loyola University Maryland, 4501 North Charles St, Baltimore, MD, 21210, United States of America

American Patent Institute, 2817 Wesleyan Drive, Churchville, MD 21028, United States of America

HIGHLIGHTS

- The Fleischmann-Pons heat effect has been verified and is nuclear.
- Ten strict conditions are necessary to achieve this effect.
- Producing a Super Abundant Vacancy Phase is the key to succeeding.
- A revised phase diagram of the Palladium – Deuterium system is employed.
- This should not be rejected as a valid topic of research, was categorically premature.

GRAPHICAL ABSTRACT

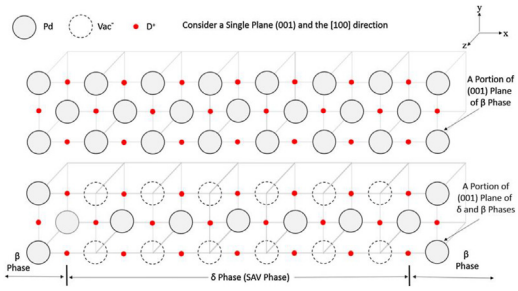

ARTICLE INFO

Article history:
Received 28 June 2022
Received in revised form
26 September 2022
Accepted 10 October 2022
Available online xxx

Keywords:
Low Energy Nuclear Reactions LENR and Cold Fusion
Palladium-Deuterium Phase Diagram and the Two Phase Region
Delta Phase and Nuclear Active Environment
Resonance Overcoming Coulomb Barrier
Conditions to Produce Fleischmann-Pons Heat Effect

ABSTRACT

To understand if cold fusion produces nuclear energy, a calorimeter was designed for electrolysis of Pd in heavy water with a precision of ± 0.5%: it exhibited excess power levels of between 20 and 240 W/cm^3 accompanied by excess heat of 150 MJ/cm^3 or 14 000 eV/atom of Pd, corroborating the original findings and verifying a nuclear source. An extra (other than commonly used Pt/H_2O) control experiment using Pd/D_2O lacked essential conditions necessary for producing the Fleischmann-Pons heat effect and so did not yield the Fleischmann-Pons heat effect, and neither did all Pt/H_2O controls. Ten hard-to-achieve but vital conditions are disclosed for a recognizable (measurable) Fleischmann-Pons heat effect; and these resulted in 100% reproducibility in this study. The phenomenon should not be rejected as a valid topic of research: it is not Rutherford's moonshine and rejection was categorically premature.

E-mail address: m.r.staker@alum.mit.edu.

https://doi.org/10.1016/j.ijhydene.2022.10.070

Please cite this article as: Staker MR, How to achieve the Fleischmann-Pons heat effect, International Journal of Hydrogen Energy, https://doi.org/10.1016/j.ijhydene.2022.10.070

Introduction

Motivation

Low energy nuclear reactions (LENR) or Lattice Assisted Nuclear Reactions (LANR) but baptized as "cold fusion" was one of three notable discoveries in late 20th century along with high-temperature superconductivity [1] and superabundant vacancy formation (SAV) [2]. Despite a hasty clandestine meeting between the father of the hydrogen bomb, Teller, and one of the discoverers, Fleischmann and Pons [3–6], and its being the subject of congressional hearings and a White House invitation; LENR was not aptly received by the scientific community, understood, nor *easily* reproduced. It was cast aside except for a resolute subgroup with curio. Berlinguette et al. [7] stated:

> "The 1989 claim of 'cold fusion' was publicly heralded… led to disqualification of the subject from further study. Motivated by the possibility that such judgement might have been premature … we describe our efforts, which have yet to yield any evidence of such an effect … [but] there remains much interesting science to be done in this underexplored parameter space **…** and additional investigation of the relevant conditions is *required* before the phenomenon can be ruled out entirely." [emphasis and "[but]" added].

They further indicate:

> "key objective of our programme was to define quantitative bounds …If *credible evidence* of an anomaly *were found*, the apparatus would be *developed into a reference experiment*." [emphasis added]

Gibney [8], regarding above, added:

> "… the project simply explored an underexplored space — *which was off limits because of prejudice,* he says. *[but] 'This is what we are supposed to do as scientists.'* …" [emphasis and "[but]" added].

Also Buchanan [9] augmented:

> "… they did find that the initial *debunking of cold fusion in 1989 was possibly premature*, as 'the relevant physical and material conditions had not (and indeed have not yet) been credibly realized and thoroughly investigated.' Today *the area remains rich in unexplained phenomena* …the subject isn't in the mainstream of current research, *but not for any particularly good reason*." [emphasis added]

Motivated by premature judgements, conditions required before ruling out, curious why reproductions failed, and to exclude prejudice; this research presents new experiments *indicating an incomplete story* as in first, third and fourth quotes. It offers reasons for ambiguity and adds perception in underexplored parameters. It suggests: the present methods, if carefully and faithfully followed, *constitute a reference experiment* previously sought in the second quote.

Background and mechanisms review

Nuclear reactions within the lattice without measurement of heat has been demonstrated. Two recent companion experimental [10] and theoretical [11] papers, did not have calorimetry, but showed nuclear reactions within the lattice. Nuclear emissions have also come from solids or ultra dense hydrogen [12–16]. Nuclear events in the lattice do not occur under the same conditions as in dilute gas phase systems. Nuclear details are incomplete, but a resonance mechanism exists [17] that overcomes the coulomb barrier. An essential phase, not known at the time of the original low energy nuclear reactions (LENR) research [3–6], was not sought, nor valued as essential in failure cases. A new phase was anticipated [18] early in LENR. The new phase, along with its parent lattice boundary, forms a nuclear active environment (NAE) actuated by resonance. Since focus was on obliging nuclear physics, within the lattice, be the same as in the dilute gas phase, conditions for *lattice* nuclear reactions have not been given adequate attention and thereby devaluating the Fleischmann-Pons heat effect. This work endeavors to mend this.

Fig. 1 shows the previously unavailable phase diagram of palladium –isotopic hydrogen (Pd – D) with delta (δ) phase centered at D/Pd = 1.33, but is extant at D/Pd = 1.14 under two-phase conditions. The δ phase is superabundant vacancy (SAV) phase with open tubes or channels for fast transport conditions. These tubes also provide conditions for resonance and for large amplitude vibrations of the deuterons [17,19,20]. Resonance is caused by normal Pd atom vibration at the end of the tube where a normally empty face centered cubic (FCC) corner position, a vacancy (Vac), is occupied by Pd (from the beta, β, phase) and the number of deuterons N in the string (in the tube) is seven with additional resonance frequencies at each additional 8 (i.e. N = 7, 15, 23, 31, …). Fig. 2 shows deuteron vibrations driven by the Pd atom from adjacent β phase whose normal thermal vibration frequency is 5.7 THz [17]. Since this is the first resonance peak, the Pd atom is the driver. Approach velocity of adjacent channel deuterons during these large vibrations in optical mode (assessed at 1.16×10^6 ms^{-1}) [17] is close to that necessary for "fusion" (some unknown nuclear event).

In SAV, vacancy (Vac) ordering is similar to gold (Au) ordering in copper–gold (Cu_3Au) alloy. In Pd, ordered SAV structures are: $Pd_3Vac_1D_x$ (δ or δ′ phases) [2,17–24] where x is 4–8, and $Pd_7Vac_1D_{6\text{-}8}$ (γ phase) [25], and result from hydrogen-induced vacancy formation [2,21,22,25–43]. Isotopic hydrogen [protium (H), deuterium (D), or tritium (T)] occupy octahedral interstitial sites (δ phase, $Pd_3Vac_1D_4$) [2,21,22] and/or tetrahedral interstitial sites (δ′ phase, $Pd_3Vac_1D_{4\text{-}8}$) [23,24]. Creation of SAV near room temperature requires a mechanism other than diffusion. This mechanism is the dragging of edge jogs connected between screw dislocations (Vac creation), followed by slight Vac relocation (attracted to D+ electromigration) to corner sites [19]. Vac have higher mobility (validated by density functional perturbation theory (DFT) [30,37–43]) from D+ electromigration, and high dislocation density promotes Vac

Please cite this article as: Staker MR, How to achieve the Fleischmann-Pons heat effect, International Journal of Hydrogen Energy, https://doi.org/10.1016/j.ijhydene.2022.10.070

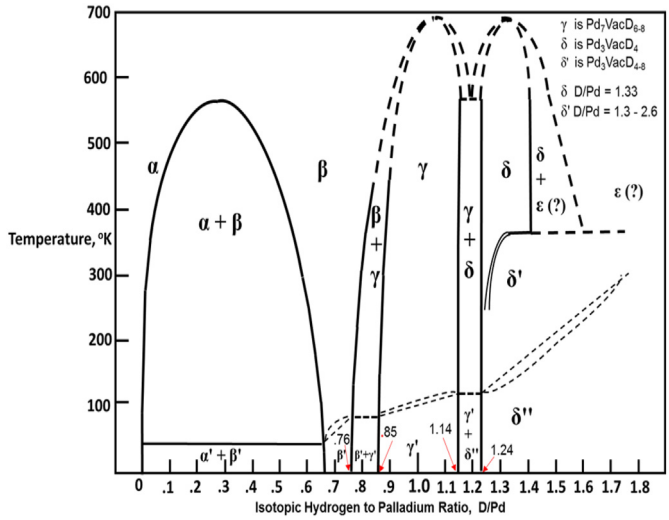

Fig. 1 – Equilibrium Phase Diagram for Hydrogen – Palladium [19,20] with SAV delta phase from 1.14 to >1.4 D/Pd ratio. In the two-phase field, the D/Pd ratio ranges from 1.14 to 1.24.

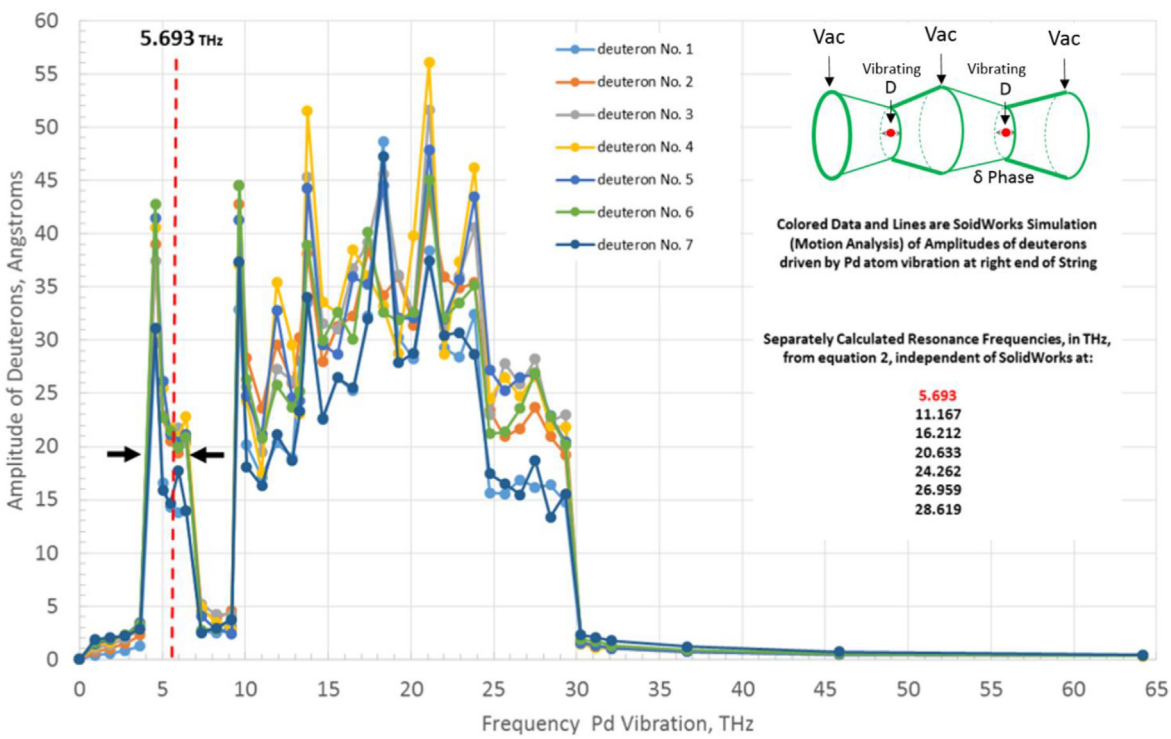

Fig. 2 – Amplitude of vibrations of seven deuterons of SAV (δ phase) due to Pd end atom at various frequencies. The first peak (m = 1) at 5.693 THz (approximate midpoint of half width) matches thermal vibration frequency of Pd (5.70 THz). If peak widths are taken into account, other peaks (2 ≤m ≤ 7) also match calculated resonance frequencies; but as m increases the peak widths overlap. Insert is the geometry of the vacancy tubes in which the deuterons vibrate and undergo resonance.

[19,44,45,46a,47]. Screw dislocation intersections during plastic deformation form edge jogs, and a string of Vac is created in the wake of moving edge jogs because their Burgers vectors are perpendicular to motion [19]. Kinetics of creation and relocation make SAV possible under room temperature electrolysis where conventional diffusion is too slow. Even so, nucleation and growth of δ to large volume fractions in the bulk by the two-step mechanism is not anticipated because of a limited supply of Vac and low kinetic rates. SAV δ phase supporting excess heat (more energy out than in) is a small volume fraction, approximately 0.03% [20]. The limited rate of creation and ordering of vacancies at room temperature and the difficulty achieving proper deuterium activity explain the incubation periods for initiating excess heat. Incubation (a

delay in the onset of excess heat) was eliminated by Szpak et al. [48,49] and Letts and Hagelstein [50] who obtained excess heat by creating Vac and SAV directly with co-deposition at high current density.

Fig. 1 represents equilibrium conditions. A mechanism is needed to nucleate δ. This mechanism is a gradient in deuteron concentration from electromigration (as in Table 1 below and Fig. 3 of Ref. [20]). This is provided by a separate current (independent of the electrolysis current). The lever rule [46b] indicates that 1.14 (left side of two-phase boundary at position 1 in Fig. 3) is the appropriate value of D/Pd ratio to cause δ to form since the volume fraction of δ is 0.03%, clearly indicating there are two phases (γ and δ or more likely β and δ, as explained in Ref. [20]). This small volume fraction allocates an ultra-short distance along the tie line [46b] into the two phase field. In other words 1.14 is the minimum D/Pd ratio to initiate two phases. Beta (or γ) has composition of 1.14 and δ has composition 1.24, but will quickly grow to 1.33 (stoichiometric). There are two means for increasing D/Pd. They are: using an independent current through Pd specimen

Table 1 – Composition enhancement from one end to the other by electromigration in Pd[a].

Total current, I (amps)	Diameter of specimen, d (cm)	Power density by joule heating, P (watts/cm^3)	Total power [= P × spec. Vol.] (watts)	Composition ratio [enhancement] C_L/C_o	
				Z = .7	Z = 1
1	.10	.175	.0035	1.10	1.14
3	.10	1.58	.0314	1.33	1.50
10	.10	17.5	.349	2.57	3.86
20	.10	70	1.40	6.60	14.91
1	.05	2.80	.014	1.46	1.72
1.5	.05	6.3	.0314	1.76	2.25
2	.05	11.2	.0559	2.13	2.95
3	**.05**	25.21	.126	**3.10**	**5.06**
10	.05	280	1.40	44.0	222.0
20	.05	1121	5.59	1902.0	49 425.0

[a] Note: Using $\rho = 10.8 \cdot 10^{-6}$ Ω-cm, L = 2.54 cm, temperature (300 K) and constant diffusion coefficient, electric wind force at zero, steady state (transient period is proportional to length^2/Diffusion coefficient, L^2/D) and no "leakage" back into electrolyte along specimen surface (highest potential). Thus, $C_L/C_o = \exp(.0005319 \cdot I \cdot L/d^2)$, for Z = 1, Joule heating (Total Power = P × Volume of specimen) uses $P = .000017\,508 \cdot I^2]/d^4$ in watts/cm^3.

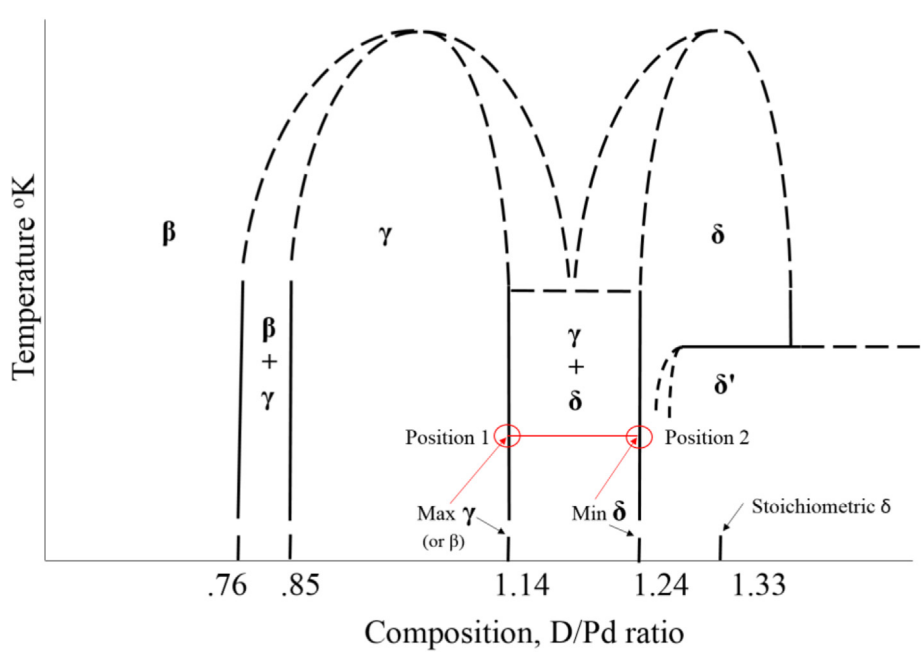

Fig. 3 – The lever rule at the red isotherm (tie line) between position 1 and 2 provide compositions of γ and δ when the overall composition (actual D/Pd ratio) is anywhere between 1.14 and 1.24, that is, the lever rule demands the composition of δ be 1.24 in the two phase region when the overal composition is somewhere between 1.14 and 1.24. Thus some delta phase will form at equilibrium when the overall local composition reaches 1.14.

Please cite this article as: Staker MR, How to achieve the Fleischmann-Pons heat effect, International Journal of Hydrogen Energy, https://doi.org/10.1016/j.ijhydene.2022.10.070

(preferred), or using a very high electrolysis current (see next section). Separate contributions (magnitudes) of the independent electromigration current I and total electrolysis current i_T are clarified in Appendix A of Ref. [20], where both contribute. It is possible to have some electromigration, if i_T is high, even if I is zero. This is not ideal since electromigration caused solely by i_T, is small, and also I serves another essential function: D/Pd ratio is determined from resistance and *requires this separate I* [19,20]. Without I there is no assurance of obtaining NAE, but it may happen. In this case reproducibility is likely to suffer. Measured resistance is the average value over Pd volume (length L of thin Pd wire, diameter d), with a gradient along the L. A specimen with measured resistance (D/Pd ratio of 0.9–1.0) allows formation of δ if the gradient augments the average D/Pd by 20% (0.95 → 1.14). Table 1 shows that probable enhancements are *multiples* of 20% (e.g. d = 0.05, I = 3, $C_L/C_o \approx 300$–500%). C_L/C_o, bottom (L) versus top (O), and is given by $C_L/C_o = \exp(4ZeI\rho L/\pi d^2 k_B T)$ where Z is ratio of D+ charge to absolute value of electron (q/|e−|), resistivity ρ, Boltzmann constant k_B and Temperature T: its derivation is in Appendix A of Ref. [19] with a transient period proportional to length^2 /(Diffusion coefficient), L^2/D. This transient is another contribution to the delayed incubation of excess heat. If electromigration takes place solely by i_T (I = 0), incubation for on-set of excess heat may be unduly prolonged, or never realized (e.g. if I = 0, i_T = 500 mA then C_L/C_o = 1.145, augmenting D/Pd by 14.5% (thus .95 →1.09) but never reaching the crucial D/Pd = 1.14).

The importance of the D/Pd ratio in achieving the Fleischmann-Pons heat effect is well established experimentally [51]: a minimum average value (threshold) is 0.88–0.90. This is shown in Fig. 4 from the work of McKubre et al. [51]. Fig. 4 is strong evidence that high average D/Pd ratio is a necessary condition to achieve the Fleischmann-Pons heat effect, and without reaching this value, independent of electromigration, one cannot expect to achieve Fleischmann-Pons heat. This points to the necessity of reliably monitoring of D activity in Pd. Monitoring of D/Pd ratio via resistance measurements generally determines the *overall* composition but does not indicate any *local enhancement* due to electromigration. Fig. 4 also shows that the higher the ratio, the more likely one will observe the Fleischmann-Pons heat effect. Berlinguette et al. [7] did not determine activity (D/Pd) in situ during calorimetry with this method. They did not observe the "hump" (local maximum) in resistance ratio (in situ resistance R divided by unloaded resistance R_o) versus loading ratio (D/Pd ≡ r_x). The method of McKubre et al. [52] and Burger et al. [53] of variation of resistivity ratio, ρ_β/ρ_{Pd} (also = to R/R_o), with r_x showing a max of 2.004 @ $r_x = 0.74$ (hump) with ρ_β obeying: $\rho_\beta/\rho_{Pd} = 0.97869 + 3.0001(r_x) - 15.090\,(r_x)^2 + 44.155\,(r_x)^3 - 49.119\,(r_x)^4 + 17.577\,(r_x)^5$; fit has correlation coefficient R^2 of 0.999. For which side of hump one is on, measurements are taken continuously, start to extant (in situ), observing rise and fall of ρ_β/ρ_{Pd} with r_x, eliminating ambiguity. Rise and fall is glaringly discernible in multiple loadings (unload anodically and reload cathodically). The purpose of multiple loadings with current density <50 mA/cm^2 and unloadings is to create plastic deformation and Vac in transitioning the miscibility gap as in Appendix B of Ref. [19]. It provides a mechanism to ratchet up loading: each reloading increases D/Pd as each cycle produces more plastic deformation and thus higher dislocation density. Resistance changes due merely to enhanced dislocation density are small compared to changes due to loading and are calibrated out using reference values, $r_x = 0$ ($R = R_o$) and $r_x = 0.74$ ($R/R_o = \rho_\beta/\rho_{Pd} = 2.004$). Initial loading (average value) is not usually above the threshold indicated in Fig. 4, however

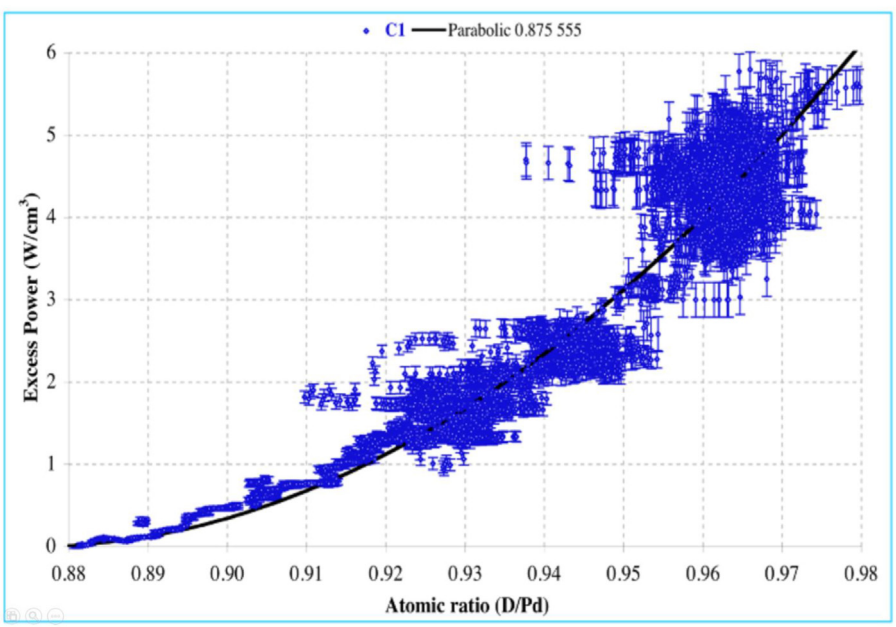

Fig. 4 – Excess Power as a function of the overall (average) D/Pd ratio, showing that the relationship is parabolic and that a minimum of the overall D/Pd ratio of .88 is needed to initiate the reaction, from McKubre et al. [51].

Please cite this article as: Staker MR, How to achieve the Fleischmann-Pons heat effect, International Journal of Hydrogen Energy, https://doi.org/10.1016/j.ijhydene.2022.10.070

the next section indicates the method to increase this to the threshold with specimen preparation. Monitoring r_x during calorimetry is the starting point for a serious effort to produce the Fleischmann-Pons excess heat.

Materials and Experimental Methods

Complete experimental details of the calorimeter are in Ref. [19], but the electrolytic cells, with Pd/D_2O (active cell) and Pt/H_2O (control cell) are shown in Fig. 5. This arrangement has the ability to measure resistivity in situ and excess heat. Nested test tubes, not shown, are described below. A Teflon top, with an O-ring seal, excluded ambient atmosphere and carbon dioxide contamination by positive pressure of O_2 and D_2 which exited a capillary tube into a reservoir of vacuum pump oil. Measurements of resistivity at constant electromigration currents I were used as described above. Voltage drop along the length L of the Pd cathode was measured outside the cell on Cu leads carrying electromigration current since 98.6% of the drop occurred in the PdD because its resistivity is 5.9–11.8 times (r_x dependent) that of Cu, however most of the voltage drop was also due to the reduced cross-section (area of Cu to PdD = d^2_{Cu}/d^2_{Pd} = 108). The effect of these two factors, along with the ratio of Cu to Pd lengths (Cu in and out of cell of 35 cm), is the final ratio of voltage drop in PdD to that of the Cu leads: it is 69.4 to 1, including the average of 5.9–11.8. The Cu leads were covered and sealed with heat-shrink electrical insulation tubes and their ends at the Pd/Cu junction were sealed with MICCROPSHIELD stop-off Lacquer from Tolber Division of Micro-Products. This technique assured the specimen (d of 0.05 cm and L of 2.54 cm) *average* D/Pd ratio was above 0.93 as in Fig. 4 before significant electromigration took place. This was arrived at after four loading cycles of repeatedly electrolytically loading, reversing polarity to unload and re-loading. This established the *average* D/Pd ratio. Then by applying the independent electromigration current I, a high deuteron concentration along with a high vacancy concentration and some δ phase were developed as indicated in Fig. 3 and Table 1.

Electromigration currents also served to balance power input to either the control (Pt/H_2O) or the active (Pd/D_2O) cell. With these balanced inputs, their outputs were also balanced unless the Pd/D_2O cell produces excess heat. Each cell's I's were controlled independently with separate power supplies. Cell voltages were not necessarily exactly the same in the two cells even though i_T was the same (they are in series) and run from another (third) power supply. Cell voltages are

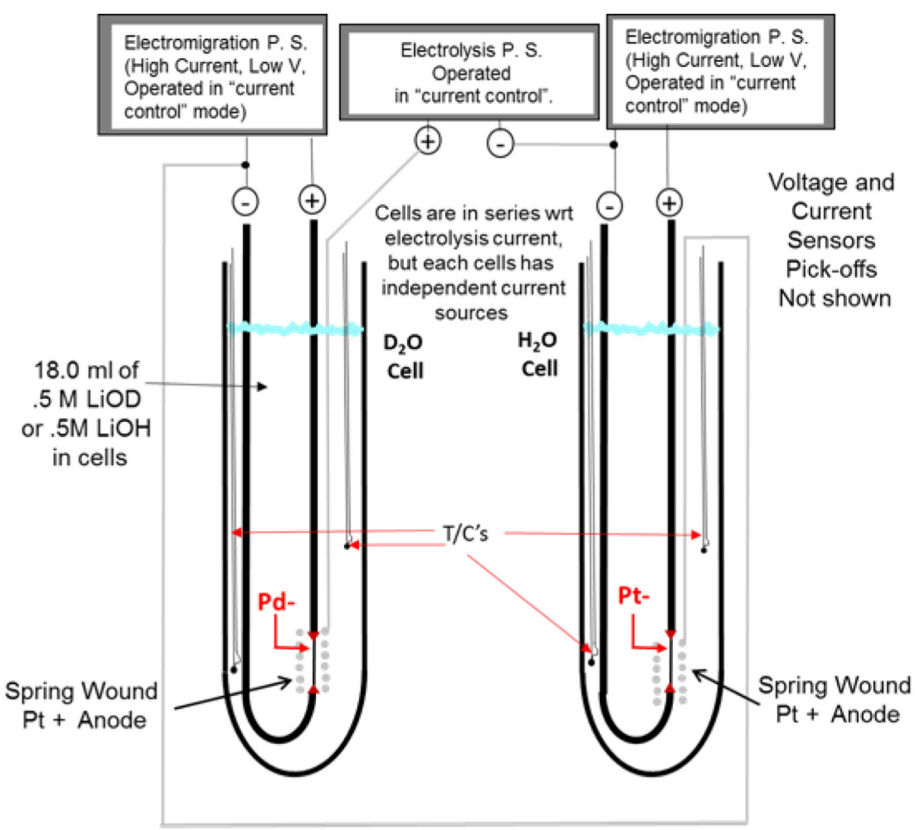

Fig. 5 – Electrolytic cells of four nested (not shown) Pyrex test tubes with Pd or Pt cathodes and Pt anodes, sealed with Teflon tops (not shown). Both cells are in series on one "current controlled" power supply (P. S.). Independent electromigration currents from P. S.'s for each cell were also operated in "current control" mode. The left cell with Pd cathode has 18 ml of 0.5 M LiOD and the right cell has 18 ml of 0.5 M LiOH, from Refs. [19,20].

Please cite this article as: Staker MR, How to achieve the Fleischmann-Pons heat effect, International Journal of Hydrogen Energy, https://doi.org/10.1016/j.ijhydene.2022.10.070

governed by i_T, anode-cathode separation distance, and electrolyte resistance (high concentration of LiOD has lower resistance and lower cell voltage). Lowering voltage by increasing the molarity of LiOD to 0.5 M (rather than the 0.1 M commonly used in other experiments) and by reducing anode-cathode distance were important to reduce input power. Reducing input power for a given i_T increased the sensitivity of the calorimeter which was an important design parameter.

Unalloyed cold worked Pd from Johnson-Matthey was used with copper (Cu) leads (5.19 mm diameter, #4 gauge wire) connected to both ends of the Pd cathode and to the plus and minus connections of current-controlled DC power supply. Attaching Cu to Pd ends, keeping the 18 ml of electrolyte from contacting Cu leads, and the complete wiring diagram for three DC power supplies are given in Figs 9, 10 and 17 respectively of Ref. [19]. Pd Expansion during D absorption was accommodated by the Cu ductility preserving the bond for the lifetime of the experiment. Pd diameter was chosen consistent with results of electromigration in Table 1 and sized to measure thermal response (consistent with ~20 Watts/cm^3) that could be distinguished from thermal output error. Twenty Watts/cm^3 was an expected output from Fleischmann-Pons papers [3–6]. Electrolysis current density at cathode surface was a key parameter in initiating, increasing, or reducing excess heat. For higher levels of excess heat a larger cell would have been required but with less sensitivity. Cells were kept small to produce as high a difference in temperature ΔT from inside to outside cell in main box calorimeter air space (Figs 11 and 15 of Ref. [19]). This design parameter is ΔT/(Power-In), the calibration slope. Precision for any given thermocouple (diameter of approximately 0.25 mm) was better than 0.05 °C since the same thermocouple repeatability does not include offset (systematic error) normally involved in absolute accuracy. Calibration eliminated offsets. A given voltage or temperature reading was determined by the average of 5000 readings collected every 0.01 s, giving an output data set every 15 min (including dead times).

Concentric Pyrex tubes (outside diameter x length of: 20 x 200, 25 x 200, 32 x 200, and 38 x 200 in mm) separated by O-rings, allowed observance of the meniscus level continuously. Delta T (ΔT) versus Power-In was calibrated before experimental runs and re-calibrated afterwards: outcomes showed no calibration shift, Figs 19 and 20 of Ref. [19]. Using four concentric test tubes caused higher ΔT for any given input. Heat transfer was largely by conduction in air gaps between test tubes. Thin air gaps minimized convection between test tubes, and close temperatures between each consecutive tube reduced radiative heat transfer because Pyrex is almost opaque at the low temperatures and the small differences in temperatures of each consecutive test tubes ("heating of car in sun" effect). Maintaining meniscus level via a Harvard Apparatus Model 22 Digital Syringe pump outfitted with two 100 ml syringes was the single most important aid to high precision since small deviations of meniscus position made large differences in measured T: details are in next section. One syringe fed heavy water (99.8% D) while a second fed double distilled light water. Since light and heavy water cells were in series, they had the same current, electrolysis rates, and rate of make-up water (set to match each electrolysis i_T rate). In addition to effects on precision, steady meniscus level kept the Pd cathode from experiencing sudden cooling spikes which were detrimental to excess heat and intolerable for staid calorimetry. Power from electromigration current (current-control mode) was product of current times voltage drop along the Pd. Electrolysis power was electrolytic current (current-control) times electrolytic voltage minus thermoneutral potential of 1.52 V for D_2O and 1.48 V for H_2O. Cell temperatures were from thermocouples (Type T used throughout this study) inside two capillary tubes (inside diameter of about 1.3 mm and outside diameter of about 2.0 mm) in each cell. An acquisition processor card 2400a by Microstar Laboratories Inc. Was used for data acquisition of voltages, and currents (measured as a voltage drop across precision resistor) for power input, and for thermocouple readings. Precision, after extensive averaging, for power-in was ± 0.0005 W, ΔT was ± 0.05 °C (or better as explained in Ref. [19]) and power-out of ± 0.015 W (based on ΔT and calibration slope). This gives overall precision of ± 0.5%.

Time constants of the cell and the constant temperature chamber (box) were in the usual way [19] yielding 34.5 min for the cell and 116 h for the chamber. The heat capacity of the calorimeter was 2500 times that of the cell. With ratio of thermal diffusivity ($\alpha = k/(\rho\ c_p)$ of air to water being 150 ($\alpha_{air}/\alpha_{water} \approx 150$) the temperature in the chamber was consistently better than if a commonly employed water bath were used. Natural convection provided constant temperature within the box (based on three thermocouples inside box). Here k is thermal conductivity, ρ is density and c_p is constant pressure heat capacity. Appendix A clarifies the ratio of cell to box time constants and its role in precision of ± 0.5%.

In preparing Pd and Pt cathodes, surfaces of Pd (or Pt) were prepared by sanding with 600 grit silicon carbide paper. Pd must contain a high dislocation density and sanding produces residual stress in the surface. After using sand paper, the surface was cleaned with aqua regia, followed quickly with distilled water, and then dried with alcohol. Care was taken not to remove significant Pd by acid dissolution and lose the residual stress zone. This improved *initial* average loading of D/Pd above 0.8.

Each cell contained a thin round horizontal Teflon baffle plate in the head-space just below the end of the tube from the syringe. This allowed Li that splashed up into the head-space (carried by D_2 and O_2 bubbles) to be washed back into the electrolyte by the incoming heavy or light water. This minimized, but not eliminated, upward cell voltage creep from diminution of concentration of Li during long time runs (decreasing sensitivity via higher parasitic input power). Pd surface contamination undoubtedly also contributed to upward creep, but this was not a problem when starting with a low initial cell voltage by using the above techniques to lower the initial cell voltage.

Ten measures, chronicled above, for NAE in Pd and to produce a recognizable (measurable) Fleischmann-Pons heat effect (next section) comprise:

Please cite this article as: Staker MR, How to achieve the Fleischmann-Pons heat effect, International Journal of Hydrogen Energy, https://doi.org/10.1016/j.ijhydene.2022.10.070

1. A high vacancy and a dislocation density (cold worked Pd with residual stress) with clean surface
2. Loading, unloading and reloading D several times to ratchet up the final *average* D/Pd ratio via plastic deformation (higher deformation is better) since previously created Vac are preserved, allowing the VAC concentration to ratchet up with each trip through the miscibility gap.
3. The net result of the above two is attaining a measured *average* threshold D/Pd ratio >0.88
4. Using a separate electromigration current for assaying D/Pd ratio and for developing a concentration gradient, using three DC power supplies (Fig. 5) thus allowing a two phase microstructure with some delta phase (*local* D/Pd ratio of 1.14) for NAE
5. Increasing the calibration curve slope (ΔT/(Power In) via nested test tubes, small size inner-most test tube, small anode to cathode separation distance, and high concentration of electrolyte (0.5 M LiOD with a baffle plate), allowing for a high electrolysis current i_T, a key enabler.
6. Stabilizing the meniscus level via a syringe pump for the make-up light and heavy water
7. Eliminating the thermal shock of manually adding make-up water via a syringe pump
8. Extensive calibration of cells before and after a run, and using a control cell in series (see method [19] of establishing a calibration curve by changing Power-In and recollecting the next data very close to the previous conditions giving a "semi-continuous curve" with ultra-precision)
9. Automatic collection of all voltages and temperatures via a data acquisition card eliminating human bias and extensive averaging (collecting every 0.01 s with 5000 readings) yielding ultra-precision.
10. Using a calorimeter with a time constant 200 times larger than that of the cell and a heat capacity of 2500 times that of the cell (provides a stable reference condition for measuring ΔT between cell and still air in calorimeter box for high precision, Appendix A)

Item 10 deals with increasing the precision of the experiment. In general, other calorimeters that are designed with a high precision (at least ± 0.5%) may provide good measurement of heat, but might be unable to have a good and constant view of the meniscus. This is essential for enabling items 6 and 7 used in an open system as described here. The others in the list stand essential on their own right.

Results and discussion

Fig. 6 shows the calibration curve (derived from Figs. 19 and 20 of Ref. [19] extended to higher power-in levels by a straight line (i.e. replacing dots of the curves, which were concave down and thus slightly lower). This is a conservative approximation. The ΔT and power-in are from various times of operation of Pd/D_2O cell during the 46-day period. There are rare scattered data below and above the calibration curve. All data below the calibration curve were taken by a data acquisition processor card under *non equilibrium* conditions: either by attempting to document effect of cell *overfilling* (electrolyte level above operating level of 18.0 ml) or when electrolysis was deliberately *stopped* briefly, allowing cell T to fall below equilibrium calibration conditions.

These periods are not part of the calibration or normal operation. At times when electrolysis is stopped, there is no excess power, and the clustered data set at the left and below the line near power-in of 2.850 W is the result of deliberately

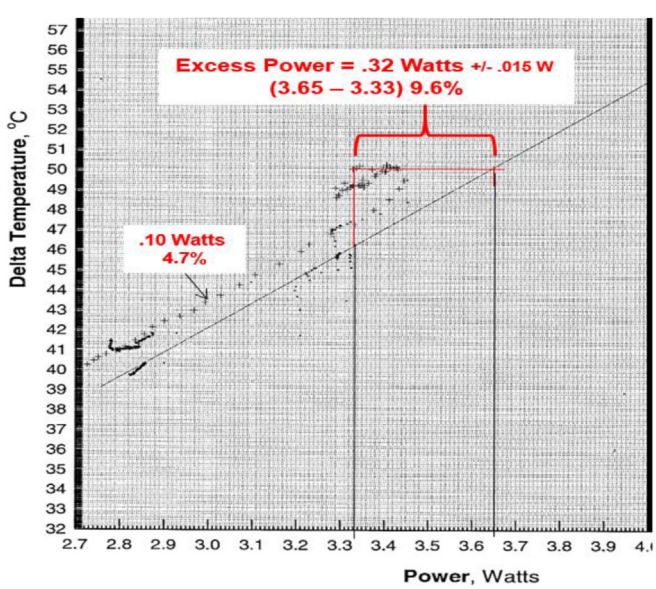

Fig. 6 – Left cell (Pd/Pt) in D_2O exhibiting excess power (*crosses*, +). The line is drawn through calibration curves of Figs. 18 and 19 of Ref. 19 (without excess heat). Excess power are above calibration curve but varied for entire 46 day period as shown by periods of 0.10 and 0.32 W excess.

Please cite this article as: Staker MR, How to achieve the Fleischmann-Pons heat effect, International Journal of Hydrogen Energy, https://doi.org/10.1016/j.ijhydene.2022.10.070

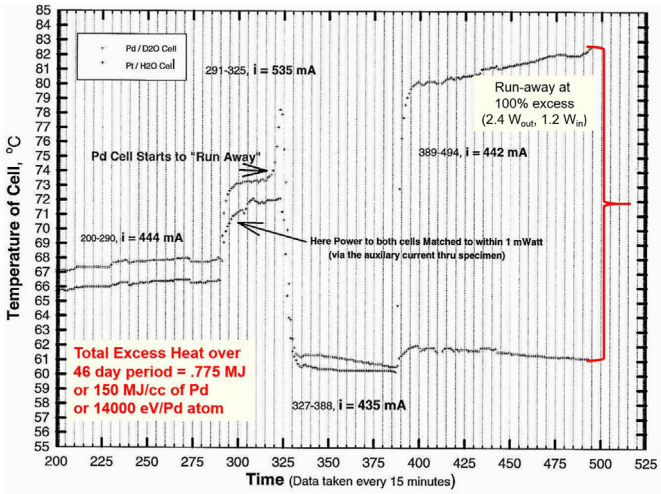

Fig. 7 – Temperatures of Pd/Pt in D_2O and Pt/Pt in H_2O cells as a function of time (one arbitrary unit on time scale represents 15 min): Pd cell is exhibiting excess power (above the control cell) and shows even more excess on sudden increase of electrolytic current. Before initiation of run-away events, power to both cells was paired to within 1 mW. Top data curve is the Pd/Pt in D_2O cell and the bottom curve is the Pt/Pt in H_2O cell.

overfilling the cell by about 1.5 mm from the equilibrium calibration mark, then allowing the electrolysis to run again without syringe pump filling. At the point where data characters (small crosses) meet the calibration line, the electrolyte level meets the 18.0 ml equilibrium level mark. This behavior was tested again at 3.290 W (tight cluster) with about 1 mm overfill and then allowed electrolysis to run until a 1 mm under-fill condition (data above line). Overfilling results in a false underestimates of ΔT (too cool) and underfilling results in false overestimates of ΔT (too hot).

All other data (crosses) above the calibration line are a result of excess power, ranging from 0.100 W (about 4.7% of power-in) to 0.320 W (9.6%). Excess power stayed in this range most of the 46 days, except for two events of run-away excess power that required cutting back i_T to prevent cell boil, Fig. 7. Excess power during run-away was triggered by increasing electrolysis current i_T, "the great enabler". Before run-away, the light and heavy water cells were matched in input power by trimming I. Power input to the cell consisted of the electrolytic power from the electrolysis current (and cell voltage) and the electromigration current (and the voltage drop along the length of the Pd cathode (for active cell) or Pt cathode (for control cell). This enabled balancing the input powers to both cell via a small change in the electromigration current to either cell, easily controlled to ± one mW. With balanced input power, any difference in cell temperature, is produced by a nuclear source of energy. The fact that the heavy water cell was hotter by 2.50 °C shows it was producing excess power. When electrolysis current i_T was increased from 444 to 535 mA and the control cell (light water) was again matched in power (via the electromigration current), the temperature of the heavy water cell started to run-away necessitating i_T be cut back to 435 mA; but excess power continued. With modest increase in current (435–442 mA), temperature ramped into run-away again, but stabilized near 82 °C, considerable higher than prior (67 °C). This second run-away event produced 2.40 W with 1.20 W input. The total excess *heat* over the 46 day period was 0.775 MJ or 150 MJ/cm^3 of Pd or 14 000 eV/Pd atom (integrating power). This is of such a magnitude that it must be nuclear; but there is no evidence which nuclear reaction.

In this study seven Pd specimens were run: six gave *excess power*, two *excess heat* similar to that reported above (150 MJ/cm^3 of Pd or 14 000 eV/Pd atom). The ones giving excess power (but not excess heat) were the result of stopping for various reasons not associated with performance – not run long enough to determine excess heat exceeding limits of chemistry. It is reasonable they would have given excess heat, since they showed the same other characteristics. Higher power densities would have resulted if i_T had not been cut back. Another specimen (seventh) had a visible longitudinal crack, and did not load properly (never exceeded 0.7 D/Pd) during the 2 weeks it ran. The reason for failing to load is given in Ref. [19]. It was used as a control experiment, verifying loading as a critical parameter. It gave no excess power or heat and was not expected to since it did not meet items 3 and 4 in the list of necessary conditions to produce the Fleischmann-Pons heat effect.

The magnitude of excess heat (Figs. 6 and 7) confirms Fleischmann–Pons heat effect from a nuclear origin. There are no chemical reactions occurring to produce heat or power since the reactants (at the start) and the products (at the end) are identical. Fleischmann and Miles [54] showed recombination is either zero or too small to be a source of heat. Excess heat per cubic centimeter of Pd (150 MJ/cm^3) or (14 000 eV/atom) is too large for a chemical reaction (which produce less than 2 eV/atom). Figs. 6 and 7 show three levels of excess

power at 0.10, 0.32, and 1.20 W, corresponding to 20, 64 and 240 W/cm^3. The excess heat produced in this research exceeded chemical energy by a factor of 7000 times (almost four orders of magnitude), indicating clearly a nuclear source. The 20 and 64 W/cm^3 were maintained for days at a time before altering input conditions. The power level of 240 W/cm^3 was deliberately terminated early to preserve the cell for recalibrate at the end of the run. The recalibration is shown in Fig. 20 of Ref. [19], where "after" run calibration data fall on top of "before" run calibration with the same precision. This research is thus a reproduction of the Fleischmann-Pons heat effect. At least one or more of the vital conditions, presented here, were missing, in whole or in part, in any failed attempts in the literature to reproduce Fleischmann-Pons heat effect. The present experimental methods, if carefully and faithfully followed, constitute a reference experiment that has been sought and is recommended for future verification by others.

Conclusions

The Fleischmann-Pons heat effect in electrolysis of Pd in heavy water at excess power levels of between 20 and 240 W/cm^3 accompanied by measured excess heat of 150 MJ/cm^3 or 14 000 eV/atom of Pd with precision of ± 0.5% is presented, verifying and collaborating the original findings and indicating the source of the energy is nuclear. An extra (other than commonly used Pt/H_2O) control using Pd/D_2O lacked essential conditions and did not yield Fleischmann-Pons heat effect, and neither did all Pt/H_2O controls. Ten hard-to-achieve but vital conditions are disclosed for a recognizable (measurable) Fleischmann-Pons heat effect; and these resulted in 100% reproducibility within this study. The phenomenon should not be rejected as a valid topic of research: this was categorically premature.

Declaration of competing interest

The author declares that he has no known competing financial interests or personal relationships that could have appeared to influence the work reported in this paper.

Acknowledgements

Without equipment and logistics support of Donald S. Hassett this research would not have been possible. Gratitude is expressed to S. Joseph and S. Anthony for their help. The author is grateful to Anthropocene Institute, Palo Alto, CA for covering the color printing cost and the article processing charge (APC) for this paper.

Appendix A. Related Box and Cell Time Constants Must Have a Large Ratio for Calorimetry Precision

A time constant is the time for temperature to change 63.2% of difference between initial (T_1) and final temperatures. The final temperature for cell and contents is $\mathbf{T_2}$ and for the Box + Air is $\mathbf{T_{BA}}$. Given an energy pulse, the temperature of cell and contents is expressed by $T = T_1 + (T_2 - T_1)\cdot[1 - \exp(-t/\tau_{Cell})]$, by definition of time constant τ_{Cell} (the heat dissipation time constant for Cell + its contents) which follows Newton's Law of Cooling (or heating). With same energy pulse, the temperature of Box + Air is expressed by $T = T_1 + (T_{BA} - T_1)\cdot[1 - \exp(-t/\tau_{Box+Air})]$, with time constant $\tau_{Box+Air}$ being the heat dissipation time constant for Box + Air. An analysis can be done using $5\cdot\tau$ instead of τ for Cell and τ for the Box yielding the same relationship of time constants. Then temperature changes 99.3% of difference between initial (T_1) and final temperatures, instead of 63.2%: both methods yield the same value for $\tau_{Box+Air}$ when it is ascertained from τ_{Cell}.

This analysis uses the measured time constant τ_{Cell} of 34.5 min to determine the *needed value of time constant of Box + Air*, $\tau_{Box+Air}$, to assure error introduced in temperature of Box + Air at the inside wall of Box does not vary enough to cause an error in measuring temperature difference between Cell contents and Air inside the Box. This error is in Fig. 1A as $\mathbf{\Delta}T_{ERROR} = T_E - T_1$. This error or variation in temperature of the Air due to a pulse of energy needs to be less than half of the minimum precision in measuring temperature of Air which is 0.01 °C, based on results of repeated cell temperature measurements during calibration. This is reported conservatively (as an overestimate) in the main body of the paper as .05 °C but it is clearly better than that for repeat measurements (precision) with the same thermocouple. Its *accuracy* is only 0.1 °C (for a thermocouple) but any *offset* involved in the accuracy can be calibrated (subtracted) out yielding the *precision* of .01 °C[1]. *Thus ratio of time constant for Box + Air is directly related to time constant of Cell + its contents for a desired precision*. This important concept is illustrated in Fig. 1A where two temperature profiles are shown as a function of time. Their respective time constants are indicated as τ_{Cell} and $\tau_{Box+Air}$.

Precision is the difference in repeat measurements of the same temperature $= T_{Now} - T_{Previous} = \Delta T = 0.01$ °C (before and after the energy pulse). If Box + Air has $\tau_{Box+Air} = \infty$ and the Box could absorb all the energy that comes to the Box instantly and the specific heat $C_p = \infty$, then $\Delta T_{ERROR} = 0$. But since $\tau_{Box+Air}$ does not $= \infty$, then ΔT_{ERROR} is finite and equal to $T_E - T_1$. The percent of $(T_{BA} - T_1)$ is small if $\tau_{Box+Air}$ is large. $(T - T_1)/(T_{BA} - T_1)$ is a percent that varies as a function of selected time t. At $t = \tau_{Cell}$, $T = T_E$ so $\Delta T_{ERROR} = (T_E - T_1)$ and $(T - T_1)/(T_{BA} - T_1) = (T_E - T_1)/(T_{BA} - T_1) = \Delta T_{ERROR}/(T_{BA} - T_1)$ and this ratio must be ½ of the precision of measurement of temperature. Thus:

$(\Delta T_{ERROR})/(T_{BA} - T_1) = (½)\cdot.01 = 1 - \exp(-t/\tau_{Box+Air})$ occuring at $t = \tau_{Cell} = 34.5$ min

$1 - .005 = \exp(-34.5/\tau_{Box+Air})$ solving for $\tau_{Box+Air}$:

$\tau_{Box+Air} = \mathbf{6883\ min} = \mathbf{115\ h} = 4.78$ days

[1] 0.01 for Appendix A purposes is conservative: a larger value (e.g. 0.05) results in $\tau_{Box+Air} = 22.7$ h which is a less demanding and a less precise calorimeter.

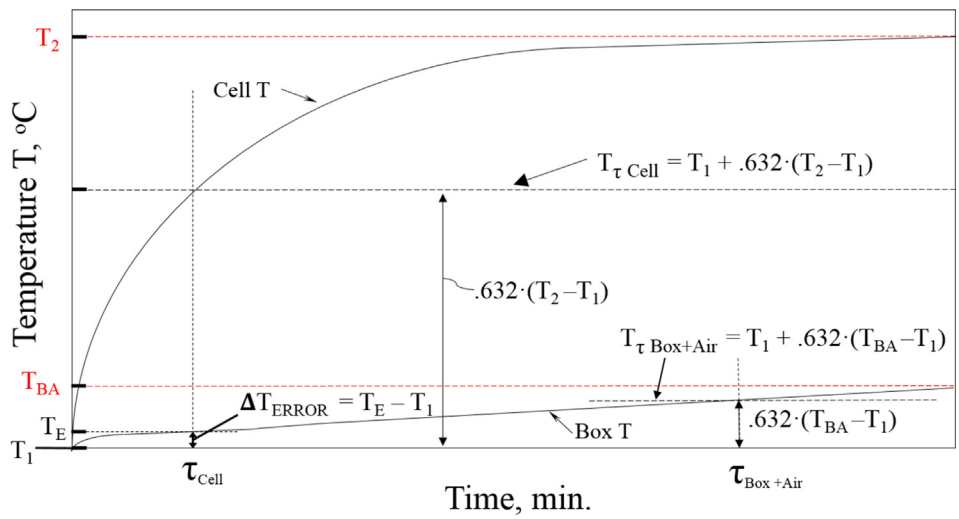

Fig 1 A – Relationship between a given Error in Temperature of Air in Box, T_E, and Time Constants of Cell and Box (solved for). This shows that ratio of time constants of Box to Cell must be large and is paramount in maintaining precision of calorimeter and measurement of temperature of air in Box. This ratio is most important design feature of calorimeter. Since $\tau_{Box\ +\ Air}$ determined here is about the same as *measured for Box* (116 h, see Materials and Experimental Methods), this analysis verifies that the precision of calorimeter is upheld exclusively by a large mass box.

REFERENCES

[1] Bednorz JG, Müller KA. Possible high TC superconductivity in the Ba-La-Cu-O system. Z Phys B 1986;64(2):189–93. https://doi.org/10.1007/BF01303701. The Nobel Prize in Physics 1987: J. Georg Bednorz and K. Alex Müller, Archived 19 September 2008 at the Wayback Machine. Nobelprize.org. Retrieved 2012-04-19.

[2] Fukai Y, Okuma YN. Evidence of copious vacancy formation in Ni and Pd under a high hydrogen pressure. Jpn J Appl Phys 1993;32:L1256–9. https://doi.org/10.1143/JJAP.32.L1256.

[3] Fleischmann M, Pons S. Electrochemically induced nuclear fusion of deuterium. J Electroanal Chem 1989;261:301–8. https://doi.org/10.1016/0022-0728(89)80141-X. errata 1989, 263, 187-189.

[4] Fleischmann M, Pons S, Anderson MW, Li LJ, Hawkins M. Calorimetry of the Palladium-Deuterium-heavy water system. J Electroanal Chem 1990;287:293–348. https://doi.org/10.1016/0022-0728(90)80009-U.

[5] Fleischmann M, Pons S. Calorimetry of the Pd-D_2O system: from simplicity via complications to simplicity. Phys Lett 1993;176:118–29. https://doi.org/10.1016/0375-9601(93)90327-V.

[6] News announcement at Univ. of Utah, 23 March 1989: https://www.youtube.com/watch?v=6CfHaeQo6oU.

[7] Berlinguette CP, Chiang YM, Munday JN, Schenkel T, Fork DK, Koningstein R, Trevithick MD. Revisiting the cold case of cold fusion. Nature 2019;570:45–51. https://doi.org/10.1038/s41586-019-1256-6.

[8] Gibney E. Google revives controversial cold-fusion experiments. Nature 2019;569:611. https://doi.org/10.1038/d41586-019-01683-9.

[9] Buchanan M. The case for cold cases. Nat Phys 2021;17:1186. https://doi.org/10.1038/s41567-021-01407-9.

[10] Steinetz BM, Benyo TL, Chait A, Hendricks RC, Forsley LP, Baramsai B, Ugorowski PB, Becks MD, Pines V, Pines M, Martin RE, Penney N, Fralick GC, Sandifer CE. II, Novel nuclear reactions observed in bremsstrahlung-irradiated deuterated metals. Phys Rev C 2020;101:044610. https://doi.org/10.1103/PhysRevC.101.044610. – Published 20 April 2020.

[11] Pines V, Pines M, Chait A, Steinetz BM, Forsley LP, Hendricks RC, Fralick GC, Benyo TL, Baramsai B, Ugorowski PB, Becks MD, Martin RE, Penney N, Sandifer CE. II, Nuclear fusion reactions in deuterated metals. Phys Rev C 2020;101:044609. https://doi.org/10.1103/PhysRevC.101.044609. – Published 20 April 2020.

[12] Holmlid Leif, Olafsson Sveinn. Spontaneous ejection of high-energy particles from ultra-dense deuterium D(0). Int J Hydrogen Energy 2015;40(33):10559–67. https://doi.org/10.1016/j.ijhydene.2015.06.116.

[13] Holmlid Leif, Kotarba Andrzej, Stelmachowski Pawel. Production of ultra-dense hydrogen H(0): a novel nuclear fuel. Int J Hydrogen Energy 2021;46(35):18466–80. https://doi.org/10.1016/j.ijhydene.2021.02.221.

[14] Roussetski AS, Lipson AG, Saunin EI, Tanzella F, McKubre M. Detection of high energy particles using CR-39 detectors Part 2: results of in-depth destructive etching analysis. Int J Hydrogen Energy 2017;42(1):429–36. https://doi.org/10.1016/j.ijhydene.2016.09.224.

[15] Mosier-Boss PA, Gordon FE, DazhuangZhou LPForsley. Detection of high energy particles using CR-39 detectors part 1: results of microscopic examination, scanning, and LET analysis. Int J Hydrogen Energy 2017;42(1):416–28.

[16] Stevenson Cheryl D, Davis John P. Hydrogen and deuterium isotope effects beyond the electromagnetic force. Int J Hydrogen Energy 2018;43(43):20011–21. https://doi.org/10.1016/j.ijhydene.2018.08.200.

[17] Staker MR. A Model and simulation of lattice vibrations in a superabundant vacancy phase of Palladium-Deuterium. Model Simulat Mater Sci Eng 2020;28:065006. https://doi.org/10.1088/1361-651X/ab9994.

[18] Bartolomeo C, Fleischmann M, Larramona G, Pons S, Roulette J, Sugiura H, Preparata G. Alfred Coehn and after: the alpha, beta, gamma of the palladium–hydrogen system, vol. 26. Lahaina, Maui, HI, USA: published by American Nuclear Society: Transactions of Fusion Technology; 1994. p. 23–47 (ISSN: 0748-1996). Also available at: *Fourth Int. Conf.*

on Cold Fusion (ICCF-4), https://www.lenr-canr.org/acrobat/EPRIproceeding.pdf. 1993, pp.19–1 to 19-47.
[19] Staker MR. Coupled calorimetry and resistivity measurements, in conjunction with an emended and more complete phase diagram of the Palladium - isotopic Hydrogen system. J. Condensed Matter Nucl. Sci. 2019;29:129–68. https://www.lenr-canr.org/acrobat/StakerMRpreprintco.pdf.
[20] Staker MR. Estimating volume fractions of superabundant vacancy phases and their potential roles in low energy nuclear reactions and high conductivity in the Palladium–isotopic Hydrogen system. Mater Sci Eng B 2020;259:114600. https://doi.org/10.1016/j.mseb.2020.114600.
[21] Fukai Y. The metal-hydrogen system: basic bulk properties. 2nd ed. Berlin, Germany: Springer; 2005. p. 216.
[22] Fukai Y, Okuma N. Formation of superabundant vacancies in Pd hydride under high hydrogen pressures. Phys Rev Lett 1994;73(12):1640–3. https://doi.org/10.1103/PhysRevLett.73.1640.
[23] Pitt MP, Gray ME. Tetrahedral occupancy in the Pd–D system observed by *in situ* neutron powder diffraction. Europhys Lett 2003;64(3):344–50. https://core.ac.uk/download/pdf/143855039.pdf accessed 25 November 2018.
[24] Ferguson Jr GA, Schindler AI, Tanaka T, Morita T. Neutron diffraction study of temperature-dependent properties of palladium containing absorbed hydrogen. Phys Rev 1965;137(2A):A483–7. https://doi.org/10.1103/PhysRev.137.A483.
[25] Fukada Y, Hioki T, Motohiro T. Multiple phase separation of super-abundant-vacancies in Pd hydrides by all solid-state electrolysis in moderate temperatures around 300 C. J Alloys Compd 2016;688:404–12. https://doi.org/10.1016/j.jallcom.2016.07.176.
[26] Oates WA, Wenzl H. On the copious formation of vacancies in metals. Scripta Met. et Mat. 1994;30:851–4. https://doi.org/10.1016/0956-716X(94)90402-2.
[27] Oates WA, Wenzl H. On the formation and ordering of superabundant vacancies in palladium due to hydrogen absorption. Scripta Met.et Mat. 1995;33:185–93. https://doi.org/10.1016/0956-716X(95)00159-S.
[28] Fukai Y. Superabundant vacancies formed in metal–hydrogen alloys. Phys Scripta 2003;2003:11. https://doi.org/10.1238/Physica.Topical.103a00011. No. T103.
[29] Fukai Y, Mizutani M. Phase diagram and superabundant vacancy formation in Cr-H alloys. Mater Trans 2002;43:1079–84. https://doi.org/10.2320/matertrans.43.1079.
[30] Tanguy D, Mareschal M. Superabundant vacancies in a metal-hydrogen system: Monte Carlo simulations. Phys Rev B 2005;72(17):174116. https://doi.org/10.1103/PhysRevB.72.174116.
[31] Fukai Y. In: Ochsner A, Murch GE, Delgado JMO\Q, editors. Hydrogen-induced superabundant vacancies in metals: implication for electrodeposition. Defect and diffusion form. Trans Tech Publications Ltd.; 2011. p. 1106–15. https://doi.org/10.4028/www.scientific.net/DDF.312-315.1106. 312-315.
[32] dos Santos DS, Miraglia S, Fruchart D. A high pressure investigation of Pd and the Pd–H system. J Alloys Compd 1999;291:L1–5. https://doi.org/10.1016/S0925-8388(99)00281-9.
[33] Degtyareva VF. Electronic origin of superabundant vacancies in Pd hydride under high hydrogen pressures. Presented conference on hydrogen materials science (ICHMS), yalta, Ukraine. August 2009. p. 25–31. http://arxiv.org/pdf/1001.1525.pdf. [Accessed 25 November 2018]. accessed.
[34] Zhang C, Alavi A. First-principles study of superabundant vacancy formation in metal hydrides. J Am Chem Soc 2005;127:9808–17. https://doi.org/10.1021/ja050475w.
[35] Fukai Y, Mizutani M, Yokota S, Kanazawa M, Miura Y, Watanabe T. Superabundant vacancy–hydrogen clusters in electrodeposited Ni and Cu. J Alloys Compd 2003:270–3. https://doi.org/10.1016/S0925-8388(02)01270-7. 356–357.
[36] Fukai Y. Formation of superabundant vacancies in M-H alloys and some of its consequences: a review. J Alloys Compd 2003:263–9. https://doi.org/10.1016/S0925-8388(02)01269-0. 356–357.
[37] Isaeva LE, Bazhanov DI, Isaev E, Eremeev SV, Kulkova SE, Abrikosov I. Dynamic stability of Palladium hydride: an ab initio study. Int J Hydrogen Energy 2011;36:1254–8. https://doi.org/10.1016/j.ijhydene.2010.06.130.
[38] Fukai Y, Sugimoto H. Formation mechanism of defect metal hydrides containing superabundant vacancies. J Phys Condens Matter 2007;19(43):436201. https://doi.org/10.1088/0953-8984/19/43/436201.
[39] Sugimoto H, Fukai Y. Migration mechanism in defect metal hydrides containing superabundant vacancies. Diffusion-fundamentals.org 2009;11(102):1–2. https://ul.qucosa.de/api/qucosa%3A13024/attachment/ATT-0/.
[40] Bukonte L, Ahlgren T, Heinola K. Thermodynamics of impurity-enhanced vacancy formation in metals. J Appl Phys 2017;121:045102. https://doi.org/10.1063/1.4974530 045102–1–045102–11.
[41] Fukai Y, Sugimoto H. The defect structure with superabundant vacancies to be formed from FCC binary metal hydrides: experiments and simulations. J Alloys Compd 2007:474–8. https://doi.org/10.1016/j.jallcom.2006.11.090. 446 – 447.
[42] Nazarov R, Hickel T, Neugebauer J. Ab Initio study of H-vacancy interactions in FCC metals: implications for the formation of superabundant vacancies. Phys Rev B 2014;89:144108. https://doi.org/10.1103/PhysRevB.89.144108.
[43] Fukai Y, Kurokawa Y, Hiraoka H. Superabundant vacancy formation and its consequences in metal hydrogen alloys. J Jpn Inst Metals 1997;61:663e670 (in Japanese), https://www.osti.gov/etdeweb/biblio/600210.
[44] Read Jr WT. Dislocations in crystals. New York, NY: McGraw-Hill; 1953.
[45] Hayden W, Moffatt WG, Wulff J. Structure and properties of materials, vol. III, mechanical behavior. New York: Wiley; 1965. p. 63–4.
[46] Reed-Hill RE. Physical metallurgy principles. Princeton, NJ: D. Van Nostrand; 1964 (a) pp.139-143, (b) p.334.
[47] Wen M, Zhang L, An B, Fukuyama S, Yokogawa K. Hydrogen-enhanced dislocation activity and vacancy formation during nanoindentation of nickel. Phys Rev B 2009;80:094113. https://doi.org/10.1103/PhysRevB.80.094113.
[48] Szpak S, Mosier-Boss PA, Smith JJ. On the behavior of Pd deposited in the presence of evolving deuterium. J Electroanal Chem 1991;302:255–60. https://doi.org/10.1016/0022-0728(91)85044-.
[49] Szpak S, Mosier-Boss PA, Dea J, Gordon F. Polarized D+/Pd-D_2O system: hot spots and mini-explosions. In: Hagelstein PL, Chubb SR, editors. Tenth international conference on cold fusion. Cambridge, MA: World Scientific Publishing Co.; 2003. p. 13–22.
[50] Letts D, Hagelstein PL. Modified Szpak protocol for excess heat. J. Condensed Matter Nucl. Sci. 2012;6:44–54.
[51] McKubre MCH, Crouch-Baker S, Riley AM, Smedley SI, Tanzella FL. Excess power observations in electrochemical studies of the D/Pd system; the influence of loading. In: Frontiers of cold fusion, third international conference on cold fusion. Tokyo, Japan: Nagoya Japan: Universal Academy Press, Inc.; 1992. p. 5–19.
[52] McKubre MCH, Rocha-Filho RC, Smedley SI, Tanzella FL, Chao J, Chexal B, Passell T, Santucci J. Calorimetry and electrochemistry in the D/Pd system, the first annual conf.

On cold fusion. Salt Lake City, Utah: Univ. of Utah Research Park; 1990. p. 20–31. National Cold Fusion Institute.
[53] Burger JP, MacLachlan DS, Mailfert R, Souffache B. Electrical resistivity of PdHx: 1 - residual resistivity. Solid State Commun 1975;17(3):277–80.
[54] Fleischmann M, Miles M. The instrument function of isoperibolic calorimeters: excess enthalpy generation due to the parasitic reduction of oxygen. Cambridge, MA: 10th Int. Conf. on Cold Fusion; 2003.

Please cite this article as: Staker MR, How to achieve the Fleischmann-Pons heat effect, International Journal of Hydrogen Energy, https://doi.org/10.1016/j.ijhydene.2022.10.070